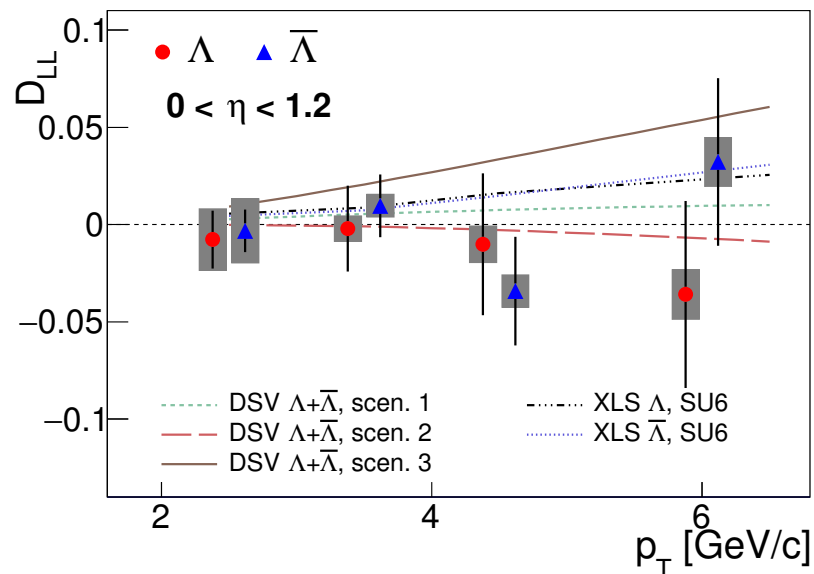


# STAR Analysis Note # 000

Longitudinal Spin Transfer of  $\Lambda$  and  $\bar{\Lambda}$  Hyperons in Polarized Proton-Proton Collisions at  $\sqrt{s} = 200$  GeV at RHIC in Run 2009



Ramon Cendejas, Jian Deng, Jincheng Mei, Ernst Sichtermann, Qinghua Xu, and Jinlong Zhang

Version 4.2 March 17, 2018

# Contents

<b>1</b>	<b>The data set</b>	<b>3</b>
<b>2</b>	<b><math>\Lambda(\bar{\Lambda})</math> reconstruction</b>	<b>3</b>
<b>3</b>	<b>Extraction of hyperon spin transfer</b>	<b>4</b>
<b>4</b>	<b>Comparison of two independent analyses</b>	<b>5</b>
<b>5</b>	<b>Results</b>	<b>8</b>
<b>6</b>	<b>Data &amp; MC comparison</b>	<b>10</b>
<b>7</b>	<b>Systematic Uncertainty Evaluation</b>	<b>10</b>
7.1	Decay parameter . . . . .	10
7.2	Beam polarization and residual transverse components . . . . .	12
7.3	Relative luminosity . . . . .	12
7.4	Residual background . . . . .	13
7.5	Trigger bias . . . . .	14
7.6	Pileup . . . . .	21
7.7	Total systematic uncertainty . . . . .	21
<b>A</b>	<b>Code documentation</b>	<b>22</b>
A.1	Analysis of data: from MuDsts to $D_{LL}$ . . . . .	22
A.1.1	Reading MuDst and producing Lambda trees . . . . .	22
A.1.2	Analysis of Lambda trees . . . . .	22
A.1.3	Extraction of $D_{LL}$ . . . . .	22
A.2	MC simulation . . . . .	22
A.2.1	Production of MC sample . . . . .	22
A.2.2	Reconstruction of $\Lambda/\bar{\Lambda}$ and $jets$ . . . . .	23
A.2.3	Analysis of the $\Lambda/\bar{\Lambda}$ and $jets$ . . . . .	23

## 1 The data set

This analysis used the  $pp$  data taken in 2009 at  $\sqrt{s} = 200$  GeV with longitudinally polarized beams at STAR. The data were reproduced with library P11id in 2012. Two triggers were selected in the analysis:

- Jet-Patch 1 (JP1) trigger with id 240410 and 240411.
- L2JetHigh (L2JetH) trigger with id 240650, 240651 and 240652.

QA for a list of runs was performed. As the hyperon analysis was done in correlation with jets and the standard jet trees from the jet group were used, the run selection started with the good run list in the jet analysis. Additional QA was applied for the JP1 and L2JetH samples for the hyperon analysis. The QA details can be found at:

[http://www.star.bnl.gov/protected/spin/qhxu/run9/QA952\\_JP1/QA\\_2009\\_952JP1.html](http://www.star.bnl.gov/protected/spin/qhxu/run9/QA952_JP1/QA_2009_952JP1.html) for the JP1 trigger and

[http://www.star.bnl.gov/protected/spin/qhxu/run9/QA952\\_L2Jet/QA\\_2009\\_952L2Jet.html](http://www.star.bnl.gov/protected/spin/qhxu/run9/QA952_L2Jet/QA_2009_952L2Jet.html) for the L2JetH trigger.

Events with primary vertices  $|Vz| < 60\text{cm}$  were selected to ensure uniform tracking efficiency. The statistics of the data sample used in this analysis is:

- 61.1M JP1 events from 769 JP1 runs.
- 28.4M L2JetH events from 819 L2JetH runs. The overlap events satisfying both the JP1 and L2JetH trigger requirements were excluded from the L2JetH sample to avoid double counting in combining the extracted spin transfers from the two sample in the end.

## 2 $\Lambda(\bar{\Lambda})$ reconstruction

The  $\Lambda(\bar{\Lambda})$  reconstruction procedure in our analysis is similar to that in the published analysis on the 2005 data[1]. The hyperon was reconstructed in the decay channel  $\Lambda \rightarrow p\pi^-$  ( $\bar{\Lambda} \rightarrow \bar{p}\pi^+$ ) with a branching ratio of 63.9%. A series of selection cuts was applied to reduce the background, and the cuts were tuned to maximize signal while keeping the residual background at the level of a few percent. The cuts were tuned independently for different intervals in hyperon transverse momentum. Table 2 has a summary.

The jet-patch trigger condition in 2009 imposed a minimum transverse energy deposit  $E_T$  (6.3GeV for JP1 and 7.8 GeV for L2JetHigh) in at least one of 18 BEMC+EEMC patches that each covered  $\Delta\eta \times \Delta\phi = 1 \times 1$  in pseudo-rapidity,  $\eta$ , and azimuthal angle,  $\phi$ . The Jet Patch trigger thus collects  $pp$  events with high transverse momentum partonic scattering. Consequently, the  $p_T$  of  $\Lambda(\bar{\Lambda})$  produced through the fragmentation of a high transverse momentum parton is expected to be on average higher than for minimum bias events. As the JP trigger is not (necessarily) caused by the  $\Lambda$  or  $\bar{\Lambda}$ , the collected event sample may be biased in a way that is different for different classes of  $\Lambda$  and  $\bar{\Lambda}$  and the effects of such biases are discussed further in Section 6. To have a better understanding of the effect to the spin transfer measurement from the trigger, we choose to focus on  $\Lambda$  and  $\bar{\Lambda}$  that are produced on the near-side of the jet, that is, the  $\Lambda$  or  $\bar{\Lambda}$  is required to be reconstructed with  $\eta$  and  $\phi$  within the jet cone of radius  $R = \sqrt{(\Delta\eta)^2 + (\Delta\phi)^2} = 0.7$  in this analysis. The jet reconstruction was done through the mid-point algorithm and the standard jet tree files for Run 9 can be found at RCF.

Cuts	(2, 3 GeV)	(3, 4 GeV)	(4, 5 GeV)	(5, 8 GeV)
TPC track hits	> 14	> 14	> 14	> 14
$dE/dx$ n( $\sigma$ )	< 3	< 3	< 3	< 3
Decay length	> 3.0 cm	> 3.5 cm	> 4.0 cm	> 4.5
DCA of $p\pi^-$ ( $\bar{p}\pi^+$ )	< 0.7 cm	< 0.5 cm	< 0.5 cm	< 0.5 cm
DCA of $\Lambda$ ( $\bar{\Lambda}$ )	< 1.2 cm	< 1.2 cm	< 1.2 cm	< 1.2 cm
DCA of p ( $\bar{p}$ )	> 0.2 cm	—	—	—
DCA of $\pi^\pm$	> 0.4 cm	> 0.4 cm	> 0.4 cm	> 0.4 cm
$\cos(\vec{r} \cdot \vec{p})$	> 0.98	> 0.98	> 0.98	> 0.98
$\Lambda$ ( $\bar{\Lambda}$ ) counts	151340 (243964)	63308 (105564)	23070 (35568)	15642 (18939)
$\Lambda$ ( $\bar{\Lambda}$ ) bkgd frac.	0.146 (0.101)	0.114 (0.081)	0.094 (0.072)	0.127 (0.115)

Table 1: Summary of the selection cuts for the  $\Lambda(\bar{\Lambda})$  reconstruction for the run9 Jet-Patch triggered sample and the corresponding  $\Lambda$  ( $\bar{\Lambda}$ ) counts and background fractions. Here “DCA” denotes the “distance of closest approach” (to the primary vertex for a single track by default),  $\vec{r}$  denotes the vector from the primary vertex to the V0 vertex, and  $\vec{p}$  denotes the momentum vector of the V0.

Fig.1a) shows the invariant mass distribution for the  $\Lambda$  (filled circles) and  $\bar{\Lambda}$  (open circles) candidates reconstructed in the near-side of triggered jet-patch with  $|\eta_{\Lambda(\bar{\Lambda})}| < 1.2$  and  $3 < p_T < 4$  GeV. The excess of  $\bar{\Lambda}$ ’s to  $\Lambda$ ’s is caused by anti-proton annihilation in the BEMC, which provides an additional energy deposit in the JP trigger compared to the  $\Lambda$  (proton) case. The residual background fraction  $r$ , is about 10% for  $\Lambda$  and 9% for  $\bar{\Lambda}$  candidates. Fig.1b) shows the same invariant mass distribution versus  $\cos \theta^*$  for  $\Lambda$ , and  $\theta^*$  is the angle between the (anti-)proton momentum in the  $\Lambda(\bar{\Lambda})$  rest frame and the  $\Lambda(\bar{\Lambda})$  polarization direction. In addition to signal and combinatorial background, a strip of misidentified  $K_s^0$  from mis-identification of the pion as a proton due to particle (mis-)identification from energy loss in the TPC can be seen at high invariant mass.

### 3 Extraction of hyperon spin transfer

In this analysis, the longitudinal spin transfer  $D_{LL}$  is extracted in a small  $\cos \theta^*$  interval as follows:

$$D_{LL} = \frac{1}{\alpha P_{\text{beam}} < \cos \theta^* >} \frac{N^+ - RN^-}{N^+ + RN^-}, \quad (1)$$

where  $P_{\text{beam}}$  is the beam polarization,  $N^+$  ( $N^-$ ) are the  $\Lambda(\bar{\Lambda})$  counts in this  $\cos \theta^*$  interval when the beam is positively (negatively) polarized, and  $R = L^+/L^-$  is the corresponding luminosity ratio for these two polarization states. The detector acceptance in this  $\cos \theta^*$  interval is taken as a constant and remains the same for both beam helicities, since the yields are measured with exactly the same apparatus in the same conditions. The detector acceptance is thus canceled. For this measurement only one polarized beam is needed. At RHIC both beams are polarized and the single spin yields  $N^+$  ( $N^-$ ) are thus formed from the yields  $n^{++}$ ,  $n^{+-}$ ,  $n^{-+}$ , and  $n^{--}$  by beam helicity configuration weighted with their corresponding relative luminosities. The luminosity ratio were determined at STAR with the BBC.

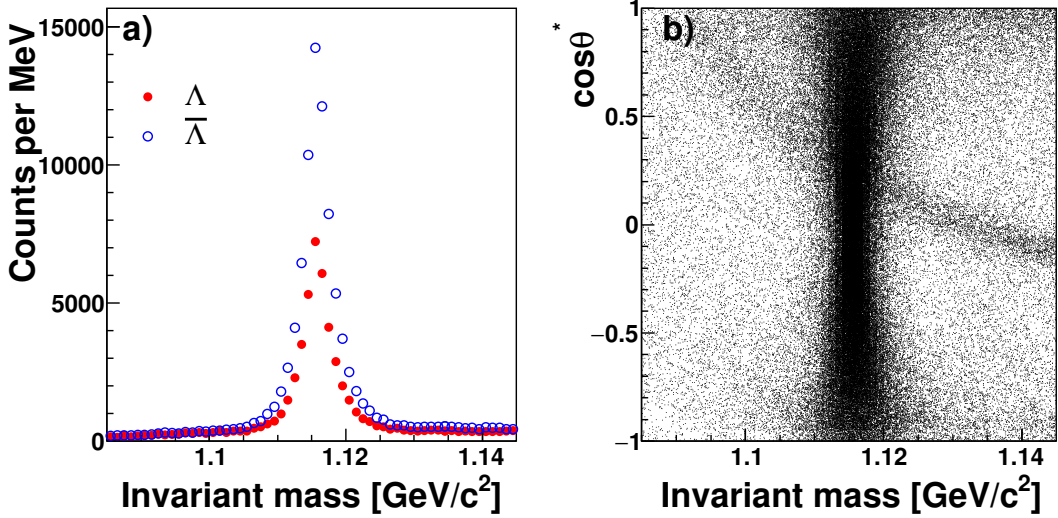


Figure 1: a) Invariant mass distribution, b) invariant mass versus  $\cos \theta^*$  for  $\Lambda$  and  $\bar{\Lambda}$  candidates with  $3 < p_T < 4$  GeV from the run 9 JP1 data sample.

The spin transfer  $D_{LL}$  was extracted for 20 intervals covering  $-1 < \cos \theta^* < 1$  as follows. First, the yields  $N^+$  and  $N^-$  were determined from the observed  $\Lambda$  and  $\bar{\Lambda}$  candidate yields in the signal region and side-band background region for each  $\cos \theta^*$  interval and the corresponding raw values  $D_{LL}^{\text{raw}}$  and  $D_{LL}^{\text{bg}}$  were extracted and averaged over the whole  $\cos \theta^*$  range. Figure 3 shows examples of  $D_{LL}$  versus  $\cos \theta^*$  for  $\Lambda$  with  $3 < p_T < 4$  GeV, including the results for a control sample of spinless  $K_s^0$ . The obtained  $D_{LL}^{\text{raw}}$  and their statistical uncertainties were then corrected for the background according to:

$$D_{LL} = \frac{D_{LL}^{\text{raw}} - r D_{LL}^{\text{bg}}}{1 - r}, \quad (2)$$

where  $r$  is the fraction of residual background under the mass peak. This fraction is typically kept below 10% to 15% for the different  $p_T$  bins in the analysis. Fig.2 gives an example of the signal and side-band region for  $\Lambda$  candidates with  $3 < p_T < 4$  GeV. The corresponding mass windows used in the side-band method are listed in Table 2. The statistical uncertainties in  $D_{LL}$  are calculated according to

$$\delta D_{LL} = \frac{\sqrt{(\delta D_{LL}^{\text{raw}})^2 + (r \delta D_{LL}^{\text{bg}})^2}}{1 - r}. \quad (3)$$

and thus contain components from dilution and subtraction. Specifically, it contains the statistical uncertainty in background  $D_{LL}^{\text{bg}}$  and the central value of the background fraction; uncertainty in the latter is taken into account as a systematic uncertainty.

## 4 Comparison of two independent analyses

The analysis of spin transfer  $D_{LL}$  has been performed by two sub-groups independently. The main difference between these two analysis comes from the selection cuts on the reconstruction

Table 2: Mass windows used in side-band estimation.

	Left side	Peak	Right side
Mass window( $\text{GeV}/c^2$ )	(1.094, 1.103)	(1.110, 1.122)	(1.129, 1.138)

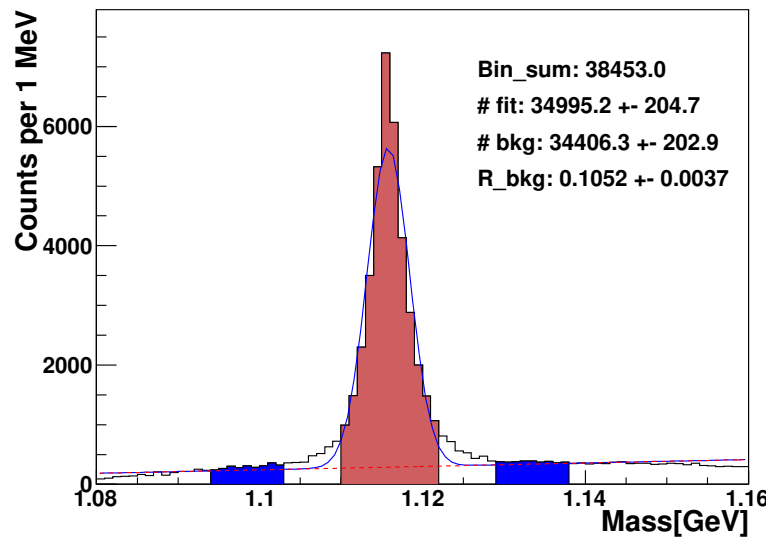


Figure 2: Invariant mass distribution for  $\Lambda$  candidates with  $3 < p_T < 4$  GeV from run 9 JP1 data sample as an example.

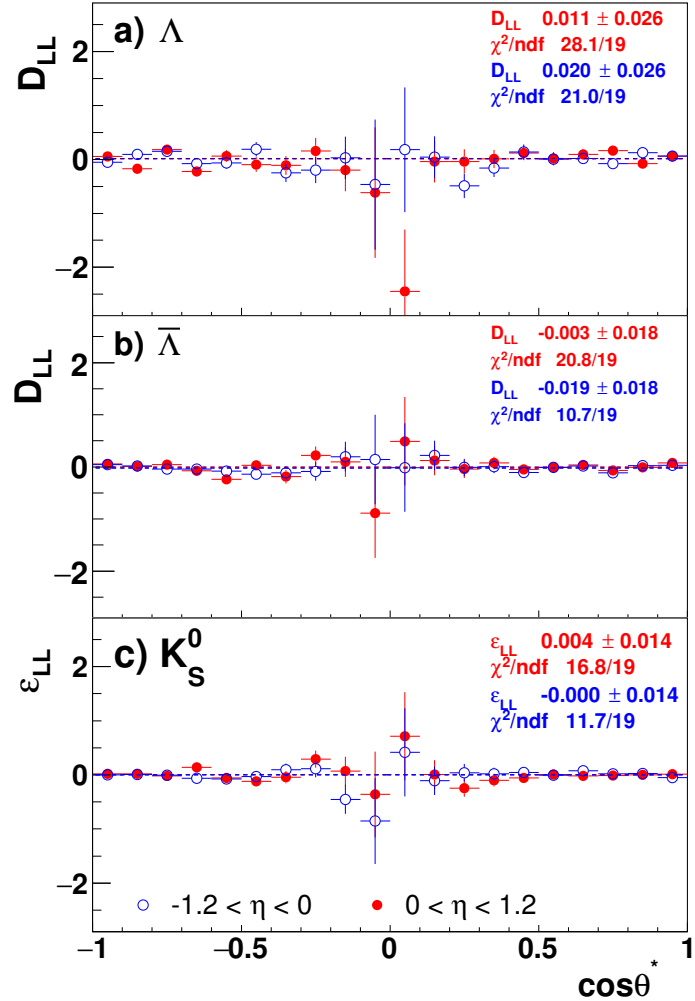


Figure 3: The spin transfer  $D_{LL}^{raw}$  versus  $\cos\theta^*$  for a)  $\Lambda$  and b)  $\bar{\Lambda}$  hyperons, and c) the spin asymmetry  $\delta_{LL}$  for the control sample of  $K_s^0$  mesons versus  $\cos\theta^*$ . The filled circles show the results for positive pseudo-rapidity  $\eta$  with respect to the polarized beam and the open circles show the results for negative eta. Only statistical uncertainties are shown.

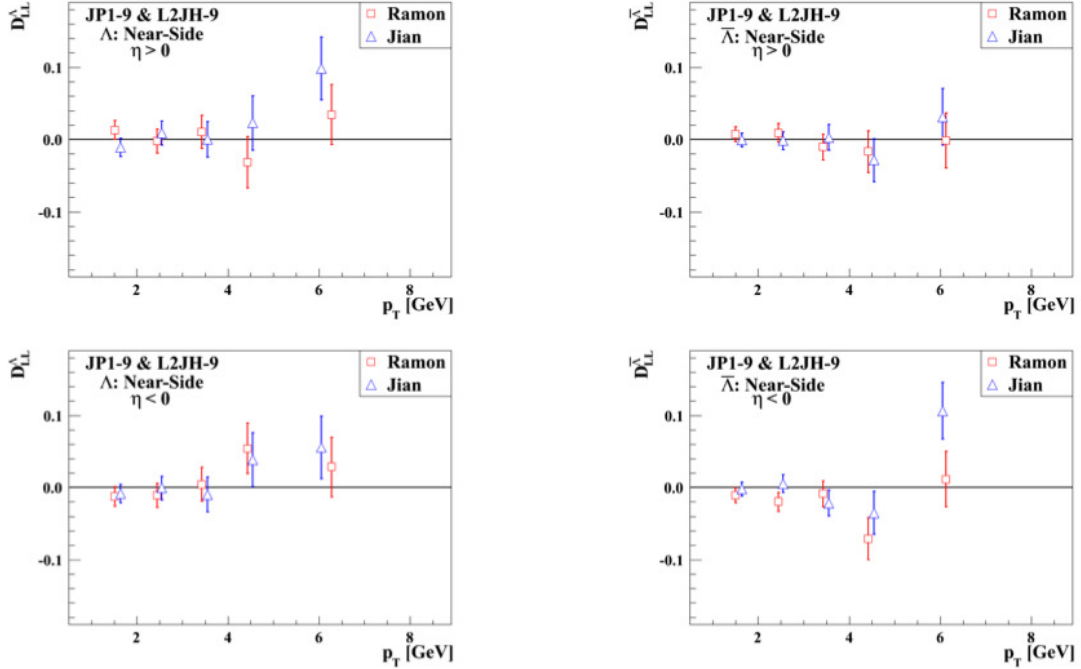


Figure 4: Comparison of two independent  $D_{LL}$  analyses using the same run9 dataset.

of hyperons. A detailed event-by-event comparison was performed for two typical runs with full magnetic field and reverse full field. The overlap region of the hyperon candidates accounts for about 50% and 65% in each analysis. The obtained final values of  $D_{LL}$  from the two analyses are compared, as shown in Fig.4. These two independent analyses give the same physics message, since the results are consistent.

## 5 Results

Events that satisfy the JP1 trigger or L2JetHigh trigger conditions were analyzed as separate samples. Events that satisfy both conditions were analyzed only as part of the JP1 sample to avoid double-counting (or correlation of the respective statistical uncertainties). Figure 5 shows the  $D_{LL}$  results for the  $\Lambda(\bar{\Lambda})$  as a function of  $p_T$  for positive and negative pseudo-rapidity with respect to the polarized beam for the JP1 and L2JetHigh samples. The  $D_{LL}$  results of  $\bar{\Lambda}$  from the JP1 and L2JetHigh samples are consistent with each other within uncertainties in the same  $p_T$  range ( $\chi^2 = 17.4/16$ ). The main results for the different triggered samples and  $p_T$  ranges are given in Table 3.

The  $D_{LL}$  results from JP1 and L2JetHigh were combined with weights determined by the point-by-point inverse statistical variance (as in an ordinary weighted average). The systematic scale uncertainties were reevaluated for the combined  $D_{LL}$  value, whereas systematic offset uncertainties were added linearly with the aforementioned weights. Fig.6 shows the combined results for positive pseudorapidity for  $\Lambda$  and  $\bar{\Lambda}$  in comparison with theoretical predictions based on different underlying models. The statistical and systematic uncertainties are shown with vertical bars

Table 3:  $D_{LL}$  results for the JP1&L2JetH merged samples with statistical and systematic uncertainties versus  $p_T$  with physics  $\eta > 0$ .

$D_{LL}$	$\Lambda$			$\bar{\Lambda}$		
	$< p_T >$	$D_{LL}$	stat	sys	$D_{LL}$	stat
2.42	-0.008	0.015	0.016	-0.003	0.011	0.017
3.42	-0.002	0.022	0.006	0.010	0.016	0.006
4.43	-0.010	0.036	0.009	-0.034	0.028	0.008
5.90	-0.036	0.048	0.013	0.032	0.043	0.013

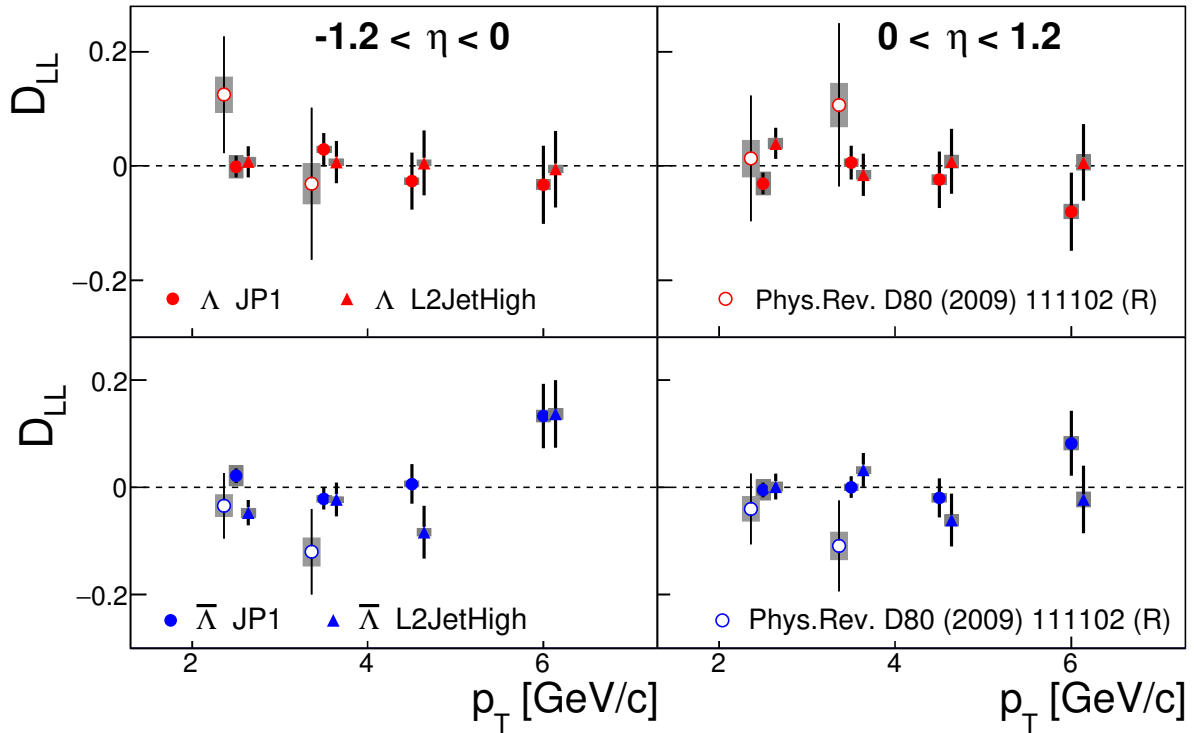


Figure 5: Comparison of spin transfer  $D_{LL}$  for differently triggered data samples for positive and negative  $\eta$  for positive and negative  $\eta$  versus  $p_T$ , also to the published Run 2005 data points. The vertical bars and bands indicate the sizes of the statistical and systematic uncertainties, respectively.

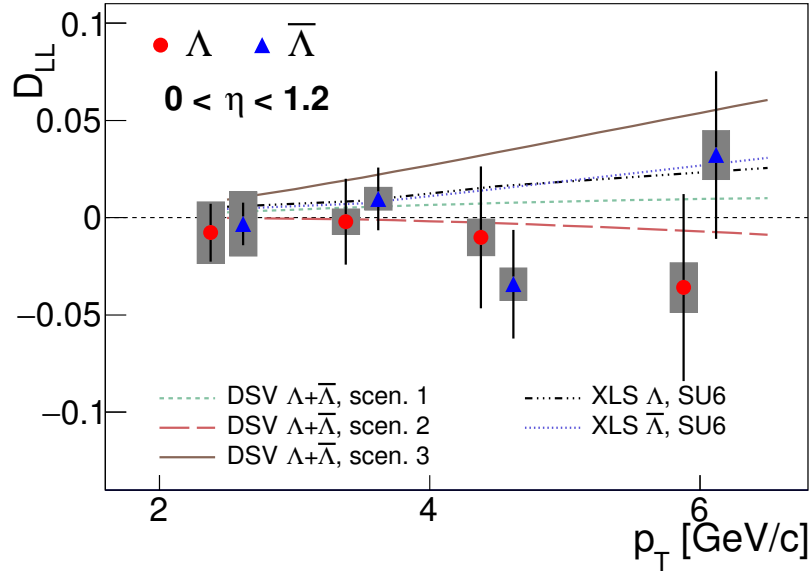


Figure 6: Comparison of the spin transfer  $D_{LL}$  with model predictions for positive  $\eta$  versus  $p_T$ . The vertical bars and bands indicate the sizes of the statistical and systematic uncertainties, respectively.

and gray bands, respectively.

## 6 Data & MC comparison

We generated MC samples with a filtered event generator, to enhance the efficiency of  $\Lambda$  and  $\bar{\Lambda}$  samples in the simulation, as we did in our previously published  $D_{LL}$  results from the run5 data. PYTHIA 6.4.28 [7] was used with a  $K$ -factor (NLO correction) of 2 to have a better description of the hyperon transverse momentum spectra. The trigger simulator for the JP1 and L2JetHigh triggers were employed in the MC samples. In general, the combined MC sample forms a good reproduction of the data for both  $\Lambda$  and  $\bar{\Lambda}$ . Fig. 7 and Fig. 8 shows the comparisons for the JP1 and L2JetHigh triggers for  $\Lambda$  as an example. Comparisons for  $\bar{\Lambda}$ , which are not shown here, are very similar for both triggers.

## 7 Systematic Uncertainty Evaluation

This section describes the systematic uncertainties we have considered for the hyperon spin transfer analysis of 2009 data.

### 7.1 Decay parameter

The decay parameter  $\alpha$  is taken from external measurements. We use the PDG value,  $0.642 \pm 0.013$ . This 2% scale uncertainty is common to the JP1 and L2JetHigh samples.

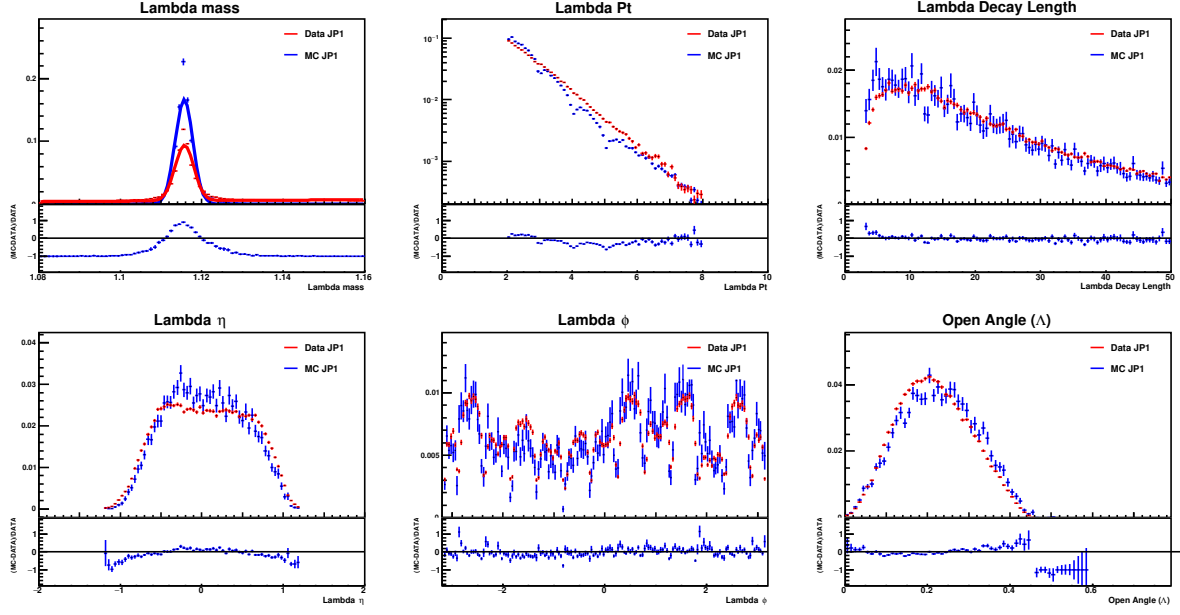


Figure 7: Data and MC comparison for  $\Lambda$  production with JP1 trigger for run9 200 GeV pp data.

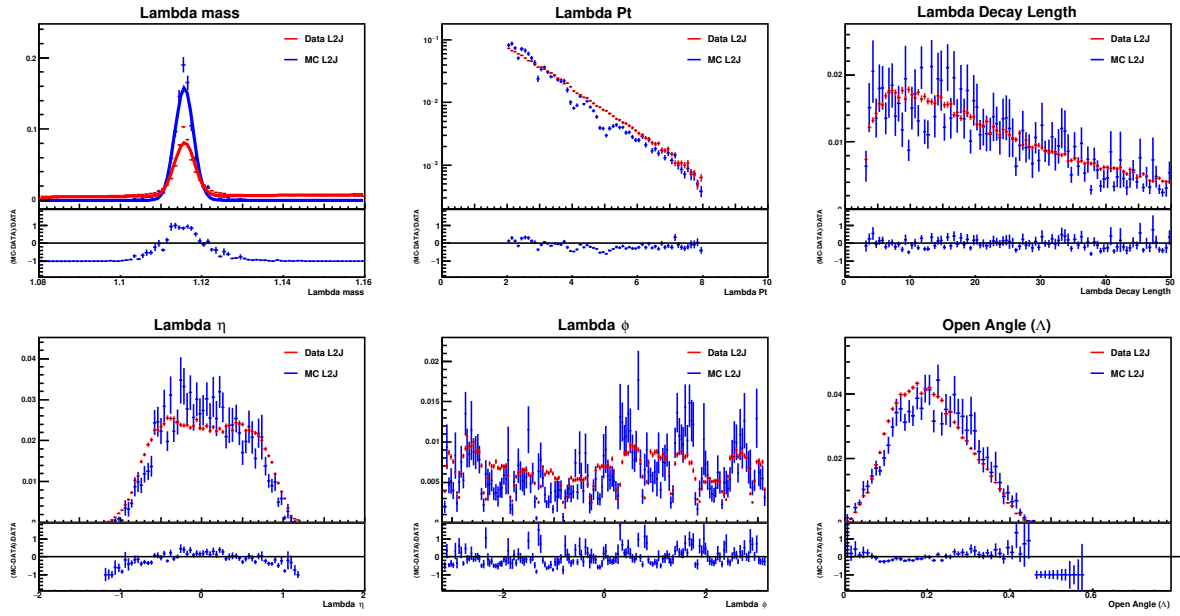


Figure 8: Data and MC comparison for  $\Lambda$  production with L2Jet trigger for run9 200 GeV pp data.

## 7.2 Beam polarization and residual transverse components

The magnitude of the beam polarizations is measured by the RHIC polarimetry group and has a 4.7% scale uncertainty (CNI official page). The analysis uses the 2009 data samples with ramped rotators at STAR and the polarization direction is thus predominantly longitudinal. The STAR BBC and ZDC were used as local polarimeters to determine residual transverse components by measuring residual single transverse spin asymmetries. The (residual) polar angles ( $\theta$ ) of the polarization direction to the longitudinal direction were found to be: 0.15 (0.25) rad for Yellow (Blue) before run 1073048, 0.13 (0.10) for Yellow (Blue) [2]. The data sample before run 10173048 amounts to 90% of the total events. We chose to work with averaged values of 0.148 for the Yellow and 0.235 for the Blue polar angles. This residual transverse component leads to two effects in terms of systematic uncertainties on  $D_{LL}$ : one is a reduction of the longitudinal polarization component at STAR from the magnitude of the polarization measured in RHIC, and the other is through the possible spin transfer from transverse beam polarization to the observed longitudinal polarization of the final state hyperon (usually called  $D_{TL}$ ). They will be dealt with separately.

- The fractional reduction of the longitudinal beam polarization was obtained from  $1 - \cos(\theta)$ , and amounts to 0.0109 (0.0275) for Yellow (Blue). The average reduction for a single beam is a relative 1.9% and behaves as a scale factor. No correction has been applied to the data, however, the size of this reduction is included in the systematic uncertainty.
- The residual transverse beam polarization is  $P_b \sin(\theta) = 0.084$  (0.133) for the Yellow (Blue) beam. Such a non-zero transverse polarization may lead to a contribution in our measurement of  $D_{LL}$  through a non-zero  $D_{TL}$  (other spin transfer components exist, however, note that we are measuring the longitudinal spin transfer).  $D_{TL}$  conserves parity, and is expected to be a higher order effect compared with  $D_{LL}$ . There are no measurements yet on  $D_{TL}$ , and it is not expected to be large. Taking into account  $D_{TL}$ , there will be an additional term to the extracted  $D_{LL}$ ,

$$dN^+ = N_{norm} \left( 1 + \alpha D_{LL} p_{beam}^L \cos(\theta^*) + \alpha D_{TL} p_{beam}^T \cos(\theta^*) \right) d \cos(\theta^*) \quad (4)$$

$$dN^- = N_{norm} \left( 1 - \alpha D_{LL} p_{beam}^L \cos(\theta^*) + \alpha D_{TL} p_{beam}^T \cos(\theta^*) \right) d \cos(\theta^*) \quad (5)$$

$$A_s = \frac{dN^+ - dN^-}{dN^+ + dN^-} \quad (6)$$

$$D_{LL} = \frac{A_s}{\alpha p_{beam}^L \langle \cos(\theta^*) \rangle} (1 + \alpha D_{TL} p_{beam}^T \langle \cos(\theta^*) \rangle). \quad (7)$$

The transverse component affects the result as a dilution effect, and the size is estimated using  $\alpha = 0.642$ ,  $|D_{TL}| < 0.1$ ,  $|p_{beam}^T| < 0.11$ ,  $\langle \cos(\theta^*) \rangle \sim 0.5$ , so the maximum shift of the  $D_{LL}$  value is  $\delta D_{LL}^{trans.pol.}/D_{LL} = 3.5 \times 10^{-3}$ . Here we take the size of  $D_{TL}=0.1$  as an upper limit, as it is a higher order effect and in the current hyperon  $p_T$  range,  $D_{LL}$  is consistent with zero within uncertainties.

## 7.3 Relative luminosity

The uncertainty in the measurement of the relative luminosity ratio  $R$  used in the extraction of  $D_{LL}$  results in an uncertainty in  $D_{LL}$ . The statistical uncertainty in  $R$  is very small on

a run-by-run basis and has been neglected. The systematic uncertainty in  $R$  was estimated using the difference between the measurements with the  $BBC$  and  $ZDC$ , and the uncertainties for different  $R$ 's are  $\delta R_4 = 1.7 \times 10^{-3}$ ,  $\delta R_5 = 2.7 \times 10^{-4}$ ,  $\delta R_6 = 1.7 \times 10^{-3}$ [3]. The same relative luminosity analysis is used as in the 2009 inclusive jet  $A_{LL}$  analysis. The corresponding uncertainty in  $D_{LL}$  has been estimated as follows:

$$D_{LL} = \frac{1}{\alpha p_{beam} < \cos(\theta^*)} \frac{\frac{N_4}{R_4} + \frac{N_5}{R_5} - \frac{N_6}{R_6} - N_7}{\frac{N_4}{R_4} + \frac{N_5}{R_5} + \frac{N_6}{R_6} + N_7}, \quad (8)$$

$$\frac{\partial D_{LL}}{\partial R_4} = \frac{-1}{\alpha p_{beam} < \cos(\theta^*)} \frac{2(\frac{N_6}{R_6} + N_7)\frac{N_4}{R_4}}{(\frac{N_4}{R_4} + \frac{N_5}{R_5} + \frac{N_6}{R_6} + N_7)^2} \frac{1}{R_4} \sim \frac{-1}{\alpha p_{beam} < \cos(\theta^*)} \frac{1}{4} \frac{1}{R_4}. \quad (9)$$

Here,  $N_{4,5,6}$  denote  $N_{++}, N_{+-}, N_{-+}$ , and  $R_{4,5,6}$  are correspondingly defined as their ratio to  $N_{--}$ . The approximation  $N_i/R_i \sim N_j/R_j$  was used to obtain the righthand side of the last expression.

The systematic uncertainty in  $D_{LL}$  caused by  $\delta R$  was estimated from,

$$(\delta D_{LL}^{rev.lum})^2 = \sum_{i=4,5,6} \left( \frac{\partial D_{LL}}{\partial R_i} \right)^2 (\delta R_i)^2 + 2 \sum_{i < j} \left( \frac{\partial D_{LL}}{\partial R_i} \frac{\partial D_{LL}}{\partial R_j} \right) Cov(R_i, R_j), \quad (10)$$

with  $Cov(R_i, R_j) = \rho(R_i, R_j) \delta R_i \delta R_j$ . The correlation is not currently known, although it is of course bound,  $-1 < \rho < 1$ . We have evaluated the uncertainty on  $D_{LL}$  using a range of correlations and (conservatively) use the maximum uncertainty thus obtained,

$$\begin{aligned} \delta D_{LL}^{rev.lum} &= \sqrt{\sum_{i=4,5,6} \left( \frac{\partial D_{LL}}{\partial R_i} \right)^2 (\delta R_i)^2 + 2 \sum_{i < j} \left( \frac{\partial D_{LL}}{\partial R_i} \frac{\partial D_{LL}}{\partial R_j} \right) \delta R_i \delta R_j} \\ &= \sum_{i=4,5,6} \left| \frac{\partial D_{LL}}{\partial R_i} \right| \delta R_i \\ &\sim \frac{1}{4 \cdot \alpha \cdot p_{beam} < \cos(\theta)} \sum_{i=4,5,6} \frac{\delta R_i}{R_i} \\ &\sim 5 \times 10^{-3}, \end{aligned} \quad (11)$$

which behaves as an additive uncertainty contribution to  $D_{LL}$  for both the JP1 and L2JetHigh sample that is constant with  $p_T$ .

## 7.4 Residual background

As mentioned earlier, the spin transfer  $D_{LL}$  is extracted using Eq.(2) considering the background subtraction. The uncertainty in the residual background is taken into account as a systematic uncertainty. The background fraction is evaluated by counting events in the side-bands, interpolating them to the signal region, and comparing them with the observed counts in the signal region. In order to estimate the systematic uncertainty caused by the uncertainty in the background estimate, the background was estimated also from a linear fit to the background and a Gaussian to describe the signal. The difference of the resulting  $D_{LL}$  values for these two methods was taken as the systematic uncertainty in  $r$ . The results are tabulated as  $p_T$  and trigger dependent offsets below.

Table 4: Systematic uncertainties on  $D_{LL}$  from residual background for near-side hyperons.

$\delta D_{LL}^{bg.}$	$\Lambda$		$\bar{\Lambda}$	
	JP1	L2JH	JP1	L2JH
$< p_T >$				
2.4 GeV	0.0005	0.0010	0.0001	0.0002
3.4 GeV	$10^{-6}$	0.0001	0.0001	0.0006
4.4 GeV	0.0007	$4 \times 10^{-5}$	0.0004	0.0002
5.9 GeV	0.0002	0.0002	0.0010	0.0001

## 7.5 Trigger bias

The data samples in the analysis are triggered for energy deposits in the EMCs, not directly on the  $\Lambda$  and  $\bar{\Lambda}$ . The trigger condition may thus introduce a bias that needs to be taken into account in either the measurement or the phenomenological interpretation of the data. We choose to account for the possible size of this effect in a systematic uncertainty in the measurements and have considered three main manifestations:

- changes in the relative contributions from different hard sub-processes and different partons in the production,
- changes in the fractional momentum  $z$  of the produced  $\Lambda$  and  $\bar{\Lambda}$  within the jet, and
- possible differences in the fraction of feed-down contributions.

We examined these changes in MC simulations before and after applying the trigger requirements using the standard STAR trigger simulator and GEANT-based simulation framework. Events were simulated using PYTHIA version 6.4.28 with tune 370.

Fig. 9, 10, 11, and 12 show the relative contributions from different subprocesses and flavors for both the JP1 and L2JetHigh trigger conditions. Based on the changes of these contributions for the different trigger conditions, we estimate the corresponding systematic uncertainties to  $D_{LL}$  using model calculations as in Ref.[4]. The values are tabulated in Table 5. We currently do not have a way to evaluate the uncertainty from process contribution in the model by De Florian et al. [5].

The distribution of the momentum fraction  $z$  before and after the JP-trigger requirement are studied for  $\Lambda$  and  $\bar{\Lambda}$  in each  $p_T$  bins with the MC sample. Here  $z$  is simply defined as the transverse momentum ratio of  $\Lambda$  ( $\bar{\Lambda}$ ) and the associated jet. Fig. 13 and 14 show the  $f_z$  distributions for different Lambda/Anti-Lambda  $p_T$  bins. Basically, the  $z$  values are shifted to smaller values by the trigger condition for moderate values of the jet  $p_T$ . This is expected. At highest jet  $p_T$ , well above the EMC thresholds, no such a reduction is found. Then with the model evaluation of  $D_{LL}$  versus  $z$  in each  $p_T$  bin, we estimate the systematic uncertainty caused by the  $z$ -shifts. Fig.15 shows the  $z$  dependent  $D_{LL}$  for  $\Lambda$  (left) and  $\bar{\Lambda}$  (right) with hyperon  $3 < p_T < 4$  GeV as an example, obtained with the model evaluations of Ref. [4].

The trigger bias contributions related with the  $z$ -shifts are tabulated below for both the JP1 and L2JetHigh samples and for each  $p_T$  value using the different models for  $D_{LL}$ . The first two

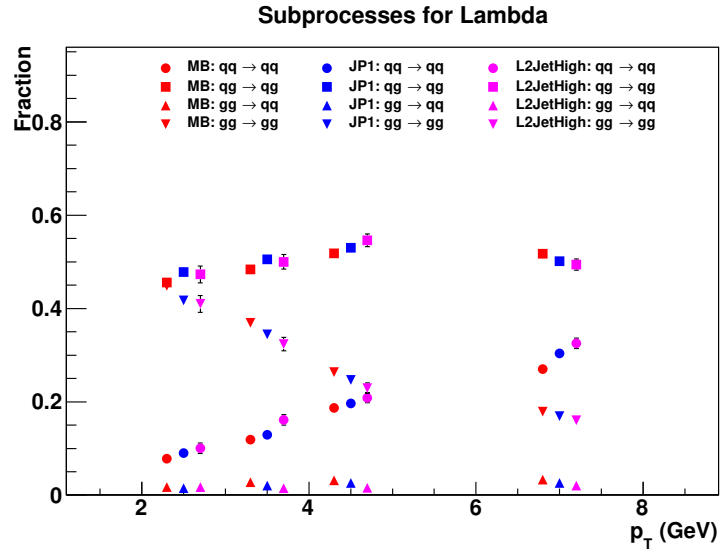


Figure 9: Subprocess fractions for  $\Lambda$  hyperons for the JP1 and L2JetHigh trigger samples in comparison to that for the min-bias trigger.

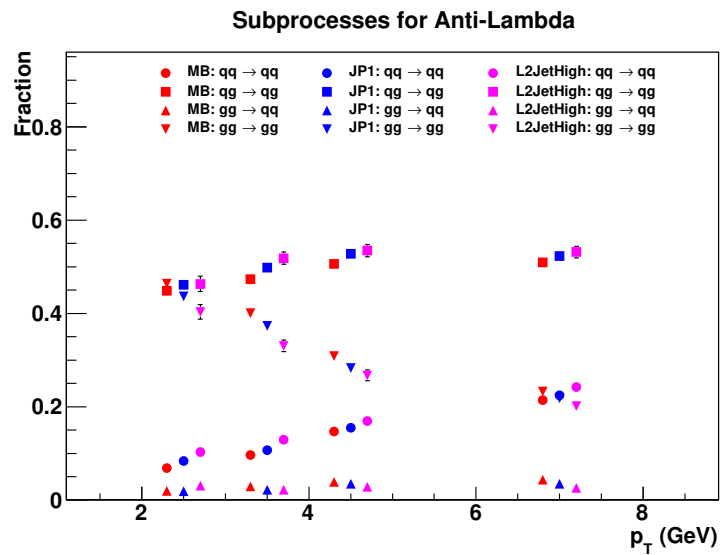


Figure 10: Subprocess fractions for  $\bar{\Lambda}$  hyperons for the JP1 and L2JetHigh trigger samples in comparison to that for the min-bias trigger.

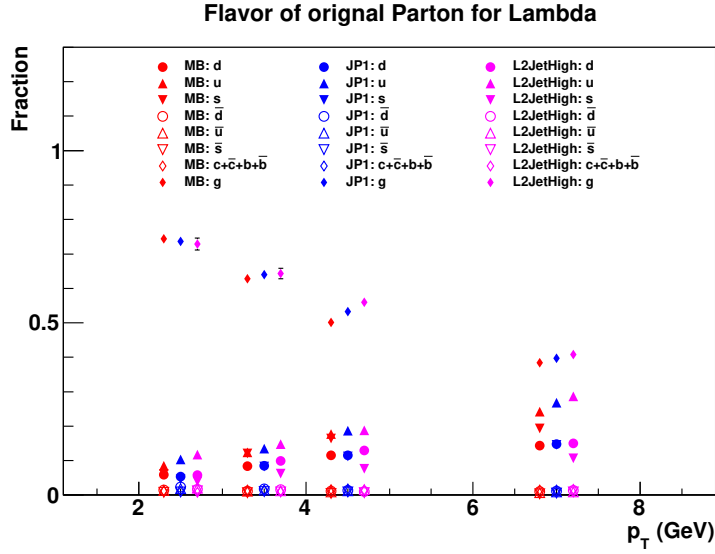


Figure 11: Fractional contributions by parton flavor for  $\Lambda$  hyperons for the JP1 and L2JetHigh trigger samples in comparison to that for the min-bias trigger.

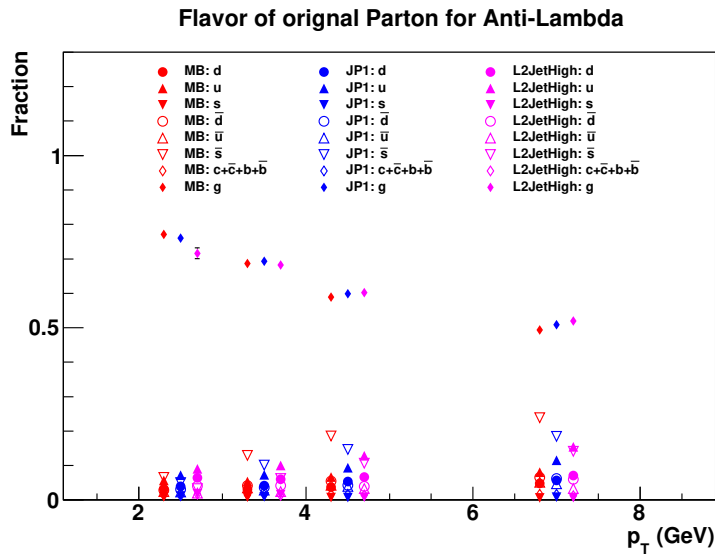


Figure 12: Fractional contributions by parton flavor for  $\bar{\Lambda}$  hyperons for the JP1 and L2JetHigh trigger samples in comparison to that for the min-bias trigger.

Table 5: Systematic uncertainties on  $D_{LL}$  caused by changes of relative contributions of subprocess and flavors with model evaluation.

$\delta D_{LL}^{sub\& flavor}$	$\eta > 0$				$\eta < 0$			
	$\Lambda[4]$		$\bar{\Lambda}[4]$		$\Lambda[4]$		$\bar{\Lambda}[4]$	
$< p_T >$	JP1	L2JH	JP1	L2JH	JP1	L2JH	JP1	L2JH
2.4 GeV	0.0005	0.0008	0.0004	0.0012	0.0001	0.0001	0.0001	0.0002
3.4 GeV	0.0011	0.0021	0.0002	0.0013	0.0003	0.0005	0.0000	0.0003
4.4 GeV	0.0019	0.0038	0.0003	0.0011	0.0005	0.0009	0.0001	0.0003
5.9 GeV	0.0034	0.0062	0.0016	0.0027	0.0011	0.0020	0.0005	0.0009

columns are obtained with model[4] for  $\Lambda$  and  $\bar{\Lambda}$  separately, and we picked the largest deviation from four inputs/models on parton distribution and fragmentation functions. This scenario basically assumes that the  $u,d$ , and  $s$  quarks contribute equally to the spin of the  $\Lambda$ , instead of the  $s$  quark contribution from the naive SU(6) picture. This scenario results in the largest  $D_{LL}$  values of all available scenarios. The polarized fragmentation function can be found in Fig. 5 of Ref.[6]. This estimate currently neglects the effect of the observed versus produced jet energy, the jet energy scale. The effect of hyperon momentum resolution (smearing) is expected to be smaller.

Table 6: Systematic uncertainties on  $D_{LL}$  caused by fragmentation momentum fraction  $z$  shift before and after the trigger condition with simulation in each  $p_T$  bin.

$\delta D_{LL}^{z-shift}$	$\eta > 0$				$\eta < 0$			
	$\Lambda[4]$		$\bar{\Lambda}[4]$		$\Lambda[4]$		$\bar{\Lambda}[4]$	
$< p_T >$	JP1	L2JH	JP1	L2JH	JP1	L2JH	JP1	L2JH
2.4	0.0009	0.0019	0.0004	0.0015	0.0000	0.0001	0.0000	0.0001
3.4	0.0026	0.0043	0.0018	0.0033	0.0001	0.0001	0.0000	0.0001
4.4	0.0055	0.0085	0.0049	0.0081	0.0006	0.0010	0.0007	0.0012
5.9	0.0069	0.0107	0.0075	0.0122	0.0014	0.0022	0.0016	0.0028

The possible effect from differences in the feed-down contributions on  $\Lambda$  and  $\bar{\Lambda}$  production were studied in simulation as well. Fig. 16 and 17 show the fractions of different feed-down contributions for  $\Lambda$  and  $\bar{\Lambda}$ , respectively. The trigger bias contributions related with the feed-down contributions are listed in Table 7 for both the JP1 and L2JetHigh samples and for each  $p_T$  value using SU(6).

The combined uncertainty from trigger-bias was estimated for each  $p_T$  interval by adding linearly the maximum of the process-contribution values and the maximum of the  $z$ -contribution values.

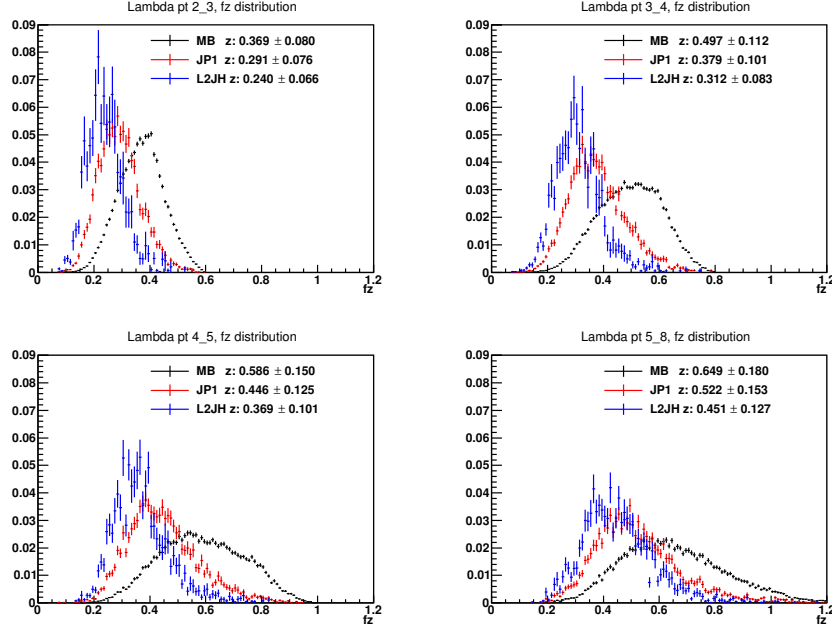


Figure 13: Fragmentation  $z$  distributions for Lambda for JP1 and L2JetHigh triggers with comparison to min-bias trigger.

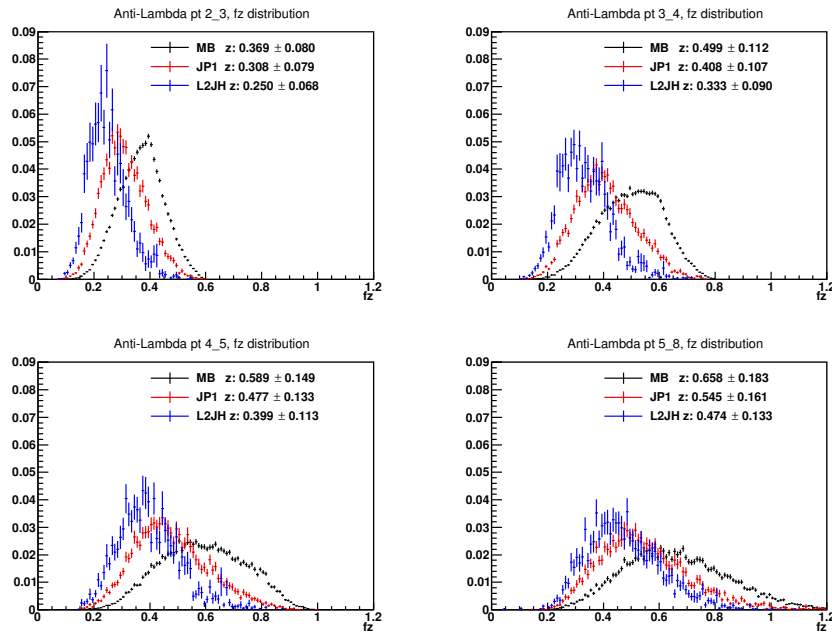


Figure 14: Fragmentation  $z$  distributions for Anti-Lambda for JP1 and L2JetHigh triggers with comparison to min-bias trigger.

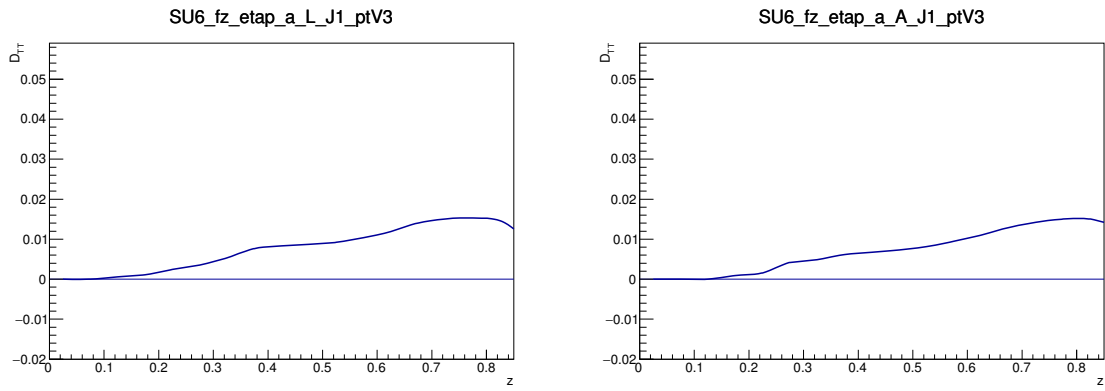


Figure 15:  $D_{LL}$  versus  $z$  for  $\Lambda$  (left) and  $\bar{\Lambda}$  (right) with  $3 < p_T < 4$  GeV from model evaluation[4].

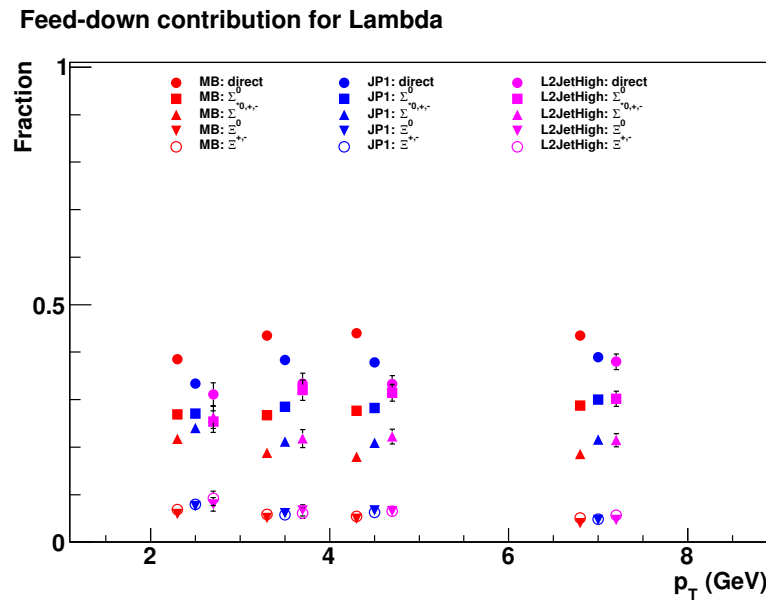


Figure 16: Feed-down contribution fractions for Lambda for JP1 and L2JetHigh triggers with comparison to min-bias trigger

### Feed-down contribution for Anti-Lambda

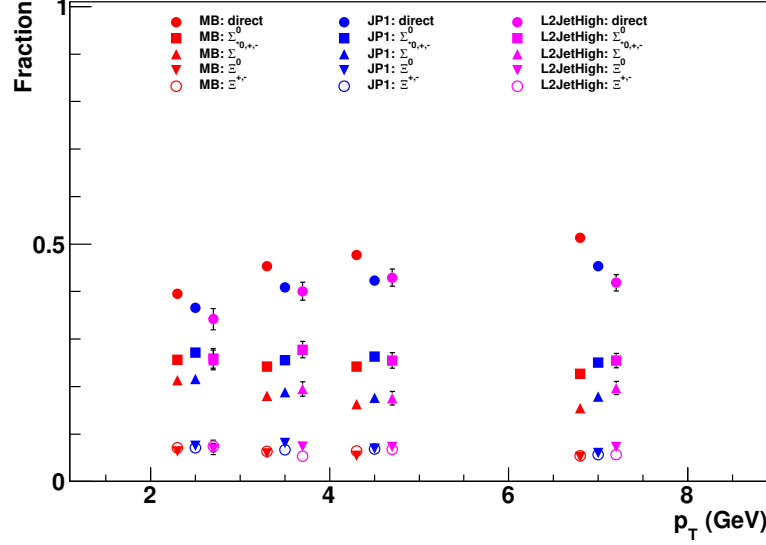


Figure 17: Feed-down contribution fractions for Anti-Lambda for JP1 and L2JetHigh triggers with comparison to min-bias trigger

Table 7: Systematic uncertainties on  $D_{LL}$  caused by changes of feed-down contributions with model evaluation.

$\delta D_{LL}^{feed-down}$	$\eta > 0$				$\eta < 0$			
	$\Lambda[4]$		$\bar{\Lambda}[4]$		$\Lambda[4]$		$\bar{\Lambda}[4]$	
$< p_T >$	JP1	L2JH	JP1	L2JH	JP1	L2JH	JP1	L2JH
2.4	0.0009	0.0018	0.0001	0.0003	0.0001	0.0000	0.0001	0.0001
3.4	0.0008	0.0011	0.0004	0.0003	0.0000	0.0001	0.0000	0.0000
4.4	0.0020	0.0027	0.0008	0.0008	0.0003	0.0004	0.0001	0.0002
5.9	0.0017	0.0024	0.0013	0.0022	0.0005	0.0009	0.0003	0.0007

## 7.6 Pileup

The effect of event-overlap was studied by spin-sorting the hyperon data sample and examining the hyperon yield per STAR event versus collision rate. This ratio is expected to be constant in the absence of pile-up. Constant and linear extrapolation to small collision rate, where pileup logically vanishes, was used to assess this systematic uncertainty contribution. Further detail may be found in Ch 3.9.5 of Ramon's thesis, which also has the values in table 3.30 on page 179. The numbers are listed in Table 8.

Table 8: Systematic uncertainties on  $D_{LL}$  from the effect of pile-up for near-side hyperons in the analysis.

$\delta D_{LL}^{pileup}$	$\Lambda$		$\bar{\Lambda}$		
	$< p_T >$	JP1	L2JH	JP1	L2JH
2.4	0.0182	0.0057	0.0184	0.0063	
3.4	0.0023	0.0007	0.0022	0.0010	
4.4	0.0023	0.0007	0.0022	0.0010	
5.9	0.0068	0.0023	0.0064	0.0023	

## 7.7 Total systematic uncertainty

The total systematic uncertainty was estimated by adding the above contributions in quadrature for each  $p_T$  interval in the analysis. This was done separately for the  $\Lambda$  and  $\bar{\Lambda}$  samples and for each trigger condition (JP1, L2JetHigh). At small  $p_T$ , pileup forms the dominant contribution, whereas trigger bias dominates the systematic uncertainty at largest  $p_T$ .

Table 9: Total systematic uncertainties for JP1 and L2JetHigh triggered sample and the combed.

$\delta D_{LL}^{all}$	$\eta > 0$						$\eta < 0$					
	$\Lambda$			$\bar{\Lambda}$			$\Lambda$			$\bar{\Lambda}$		
$< p_T >$	JP1	L2JH	comb	JP1	L2JH	comb	JP1	L2JH	comb	JP1	L2JH	comb
2.4	0.0196	0.0084	0.0159	0.0191	0.0083	0.0165	0.0195	0.0077	0.0157	0.0191	0.0085	0.0164
3.4	0.0062	0.0071	0.0065	0.0058	0.0065	0.0059	0.0057	0.0051	0.0055	0.0056	0.0053	0.0055
4.4	0.0084	0.0109	0.0094	0.0075	0.0102	0.0084	0.0058	0.0052	0.0055	0.0055	0.0070	0.0056
5.9	0.0123	0.0138	0.0128	0.0122	0.0139	0.0126	0.0088	0.0063	0.0075	0.0111	0.0098	0.0104

## A Code documentation

The code used in this analysis is (*will be*) checked into CVS under offline/paper/psn *ToBeAssigned/*.

### A.1 Analysis of data: from MuDsts to $D_{LL}$

#### A.1.1 Reading MuDst and producing Lambda trees

Currently, the muDst files for run9 are not available on RCF disk any longer. For test, one can always download a small number of mudst files from HPSS. The file list can be accessed via catalog:

```
get_file_list.pl -keys path,filename -cond production=P11id,trgsetupnameProduction2009_200GeV,filetype=daq_reco_MuDst,storage=hpss -limit 0
```

For reading the MuDst files (when the data is on the disk), you can just go inside directory muDst2LamJetTree/, compile, and run the executable file Run\_job.x, after which the analysis jobs will be submitted. The output files – the Lambda trees can be found in the scratch directory \$USER/..

```
cd Data/muDst2LamJetTree/
cons
Run_job.x
```

#### A.1.2 Analysis of Lambda trees

```
cd Data/LamReco/scheduler/
submit.csh
```

#### A.1.3 Extraction of $D_{LL}$

```
cd exDLL
1_runmerge.csh
2_runfit.csh
3_exdll.csh
```

## A.2 MC simulation

### A.2.1 Production of MC sample

This is the most time-consuming part of the MC simulation. In directory MC/, there are codes, input run lists, and the script to submit the MC production running jobs to the RCF cluster.

```
cd MC/Generator/scheduler/
```

The `.sh` and `.xml` files should be appropriately modified. Then you can submit the jobs executing:

```
Run_gen.csh
```

Then, the output files including `MuDst.root`, `geant.root`, `event.root` files can be found in the directory set in the `.sh` script.

### A.2.2 Reconstruction of $\Lambda/\bar{\Lambda}$ and jets

In this step, the consistent jet and  $\Lambda$  reconstruction algorithms are used.

```
cd MC/Reconstruction/  
cons  
Run_job.csh
```

Note, the arguments inside the `.csh` and `.xml` scripts should be appropriately modified as needed.

### A.2.3 Analysis of the $\Lambda/\bar{\Lambda}$ and jets

In above two steps, all the MC events are generated for individual partonic  $\hat{p}_T$  bins. Now, we need to merged them together.

```
cd MC/Analyzer/merge/  
Run_job.csh
```

The weight for each  $\hat{p}_T$  interval is calculated from **generated events / cross section** which can be found from the log files of the first step (events generation). The input weight numbers should be modified in subdirectory `weight_ptH/`.

Finally, all histograms needed for extracting the trigger bias will be filled.

```
cd MC/Analyzer/toHist/  
Run_job.csh
```

As usual, the `.csh` and `.xml` scripts should be appropriately modified as needed.

Now, all the needed histograms are produced. The trigger bias can be extracted by using a few short macros. In `TriggerBias/` directory, the macros used in this analysis can be taken as reference.

Overall, this codes mentioned in this section are not professional enough. If any confusion are met, please feel free to contact Jincheng Mei (`jcmei@rcf.rhic.bnl.gov`) and Jinlong Zhang (`jlzhang@rcf.rhic.bnl.gov`).

## References

- [1] B.I. Abelev *et al.* [The STAR Collaboration], Phys. Rev. D**80**, 111102 (2009).
- [2] Oleksandr Grebenyuk, “Local Polarimetry in Run 9”, STAR talk
- [3] Joe Seele, “Local An update on the run9 pp200 rellumi analysis - part deux”, STAR talk
- [4] Q.H. Xu, Z.T. Liang and E. Sichtermann, Phys. Rev. D**73**, 077503 (2006).
- [5] D. de Florian, M. Stratmann and W. Vogelsang, Phys. Rev. Lett. **81**, 530 (1998), and private communication.
- [6] D. de Florian, M. Stratmann and W. Vogelsang, Phys. Rev. D. **57**, 5811 (1998).
- [7] T. Sjostrand, S. Mrenna, and P. Skands, J. High Energy Physics **2006.05** (2006) P.026.
- [8] Ramon Cendejas, PhD. Thesis (2012), UCLA,  
[http://drupal.star.bnl.gov/STAR/files/ramonCendejas\\_Thesis\\_1.pdf](http://drupal.star.bnl.gov/STAR/files/ramonCendejas_Thesis_1.pdf).